PZT-ACTUATED COMPLIANT LOCKING DEVICE

Martin Tschiersky[1], Giovanni Berselli[2], Just L. Herder[3], Dannis M. Brouwer[1] and Stefano Stramigioli[4]

[1]Chair of Precision Engineering
University of Twente
Enschede, The Netherlands

[2]Department of Mechanics, Energetics, Management and Transportations
University of Genoa
Genova, Italy

[3]Department of Precision and Microsystems Engineering
Delft University of Technology
Delft, The Netherlands

[4]Department of Robotics and Mechatronics
University of Twente
Enschede, The Netherlands

Abstract

In this paper, a novel design of a fully compliant locking device is presented, for possible application in robotic actuation systems. The synthesis method based on a rigid linkage mechanism is explained, a parametrization scheme is proposed, and an optimization procedure is conducted using kinetostatic flexible multi-body analysis in conjunction with global optimization techniques. The performance of the optimized locking device design is validated via numerical simulations.

INTRODUCTION

Locking devices can be subdivided into several subclasses, such as clutches and brakes. Commonly, these machine elements rely on the contact between friction surfaces for their functioning.

Friction-based Locking Devices (FLDs), along with other types of mechanical and singularity-based lockers [1], have been applied in robotics and mechatronics applications with the aim of increasing energy efficiency, improving safety or to reconfigure modular assemblies.
With respect to energy management, the FLDs main function is either to reduce the actuators energy consumption during standstill by disconnecting the load (e.g. normally-closed brakes installed on industrial robots) or to control the power flow of elastic energy buffers employed in advanced actuation systems, such as series-elastic [2], parallel-elastic [3] or variable stiffness actuators [4]. A structured method to analyze clutched elastic actuator designs is presented in [5].

A large number of FDL designs have been presented and commercialized, which can be compared on the basis of a set of desirable technical characteristics [6]. In particular, FLDs should be compact, lightweight and guarantee a short switching time between the locked and unlocked state, while simultaneously providing a high maximum locking torque.

One potential means of achieving these properties in a FDL for rotary applications is the use of piezoceramics, namely lead zirconate titanate (PZT), for actuation. PZT-stack actuators offer a large bandwidth as well as a high specific power. Furthermore, their capacitive nature results in lower energy consumption in comparison to other actuation principles. The idea of a piezoelectric actuated brake was first patented in 1989 by Yamatoh et al. [7] and was also used in the patented actuator of Hanley et al. [8].
The main challenge associated with the use of piezoelectic materials for applications beyond the micrometer scale lies in their low-displacement and high-force characteristic. Therefore, generally a transmission mechanism for displacement amplification is necessary.

The goal of our research is to leverage the advantages while overcoming the challenges of piezoelectric actuation in a novel compliant locking mechanism, to be used for both clutch and brake applications. While many linear single-stage PZT motion amplifiers have been conceived in the past [9], this paper presents a novel inherently radially coupled multistage concept.
First, the design synthesis is presented. In the following sections the design topology is parameterized and the geometry is optimized. The performance of the optimized result is validated via numerical simulations across different software packages. Lastly, the results are discussed and conclusions elaborate on the main findings.

CONCEPT

The proposed mechanism, though different in its technical nature, is inspired by the functional principle of the planar Hoberman linkage [10]. A small radial stroke at the outside of the mechanism is converted into a largely amplified radial stroke at its inside. Thus, a small actuator displacement at the outer perimeter can be used to clamp a shaft which is located at the center of the mechanism. In contrast to a mechanism with the same mechanical advantage but only one point of engagement, the proposed mechanism, similarly to the Hoberman linkage, engages to the shaft at symmetrically spaced points around the rotation axis. Thus, the reaction forces due to the normal forces at the contact are contained within the mechanism itself.

Still, when using PZT-actuators, the input displacements are typically at an order of magnitude at which any backlash in the system leads to a rapid functional degradation. Therefore, a monolithic flexure mechanism is proposed, in which the desired kinematics are achieved purely by elastic deformation, that is mainly by bending of its compliant members. The design topology is obtained by conceptually converting a linkage system, that is solely comprised of rigid members and revolute joints, into a corresponding fully compliant mechanism, which is suitable for parameter optimization. The three-step synthesis process is illustrated in Figure 1.

Rigid link concept

In the basic concept, shown in Figure 1 a), a number of output nodes $n_n \geq 3$ is equally distributed on an inner pitch circle with radius r. Radially adjacent output nodes connect to each other via two rigid links of equal length l that are connected to another by a second set of revolute joints. Thereby, the loop of the first amplification stage is closed. Based on the terminology of Hoberman [10], we will refer to the inner nodes of a stage as central nodes and to the outer ones as terminal nodes. Radial lines passing through the central node of the first stage will be referred to as unit lines and the ones passing through the terminal points as normal-lines. The angle between two normal-lines will be referred to as the normal angle $\alpha = {}^{2\pi}/_{n_n}$. The sections between two normal-lines constitute the unit cells of the mechanism.

The terminal nodes of the amplification stage again form a concentric circle and in turn constitute either the input of the entire mechanism or the output, i.e. the central nodes, of a consecutive amplification stage. The total number of consecutive stages n_s can be any positive integer. The normal angle α of the mechanism is preserved as long as the mechanism input displacement at the outer perimeter is radially symmetric.

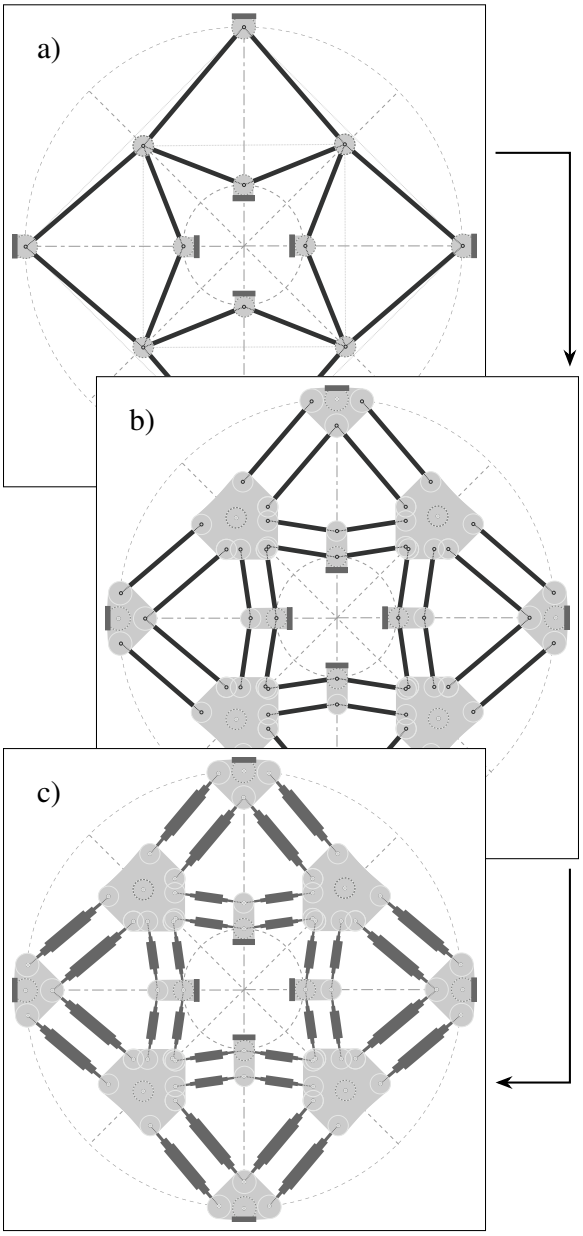

FIGURE 1. Synthesis of the mechanism topology for $n_n = 4$ and $n_s = 2$. Pitch circles and normal-lines are depicted by light gray dashed lines, the unit lines by dash-dotted lines and the singularity lines by dotted lines. Rigid bodies are illustrated by gray areas, rigid links by dark gray thick lines and the compliant links by medium dark gray lines with changing thickness.

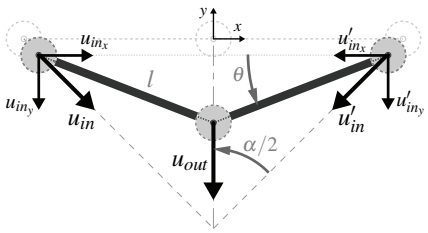

FIGURE 2. Unit cell kinematics.

Unit cell

The function principle of each unit cell is similar to that of a toggle lever. Assuming a symmetric translational input u_{in} along the normal-lines at both terminal nodes, the central node will travel along the unit line. In order to avoid a singular configuration of the mechanism, the central nodes and terminal nodes must not lie in a straight line. Thus, an angle θ between the links and the straight line is formed. An example of a single unit cell is illustrated in Figure 2. The output displacement u_{out} is given by:

$$u_{out} = lsin\theta + u_{in}cos\frac{\alpha}{2} \tag{1}$$

From Equation 1 it can be seen that the output motion is a superposition of the linear motion $u_{in}cos\frac{\alpha}{2}$ and the non-linear motion $lsin\theta$. The latter being the characteristic motion, which is leveraged in order to obtain a very high initial ratio (infinite at $\theta = 0$) to travel from the initial position to the contact position and to produce a lower ratio for transmitting normal forces to the shaft, when in contact. Plots of the output displacement u_{out}, as well as for the transmission ratio in relation to the input displacement u_{in} and to the normal angle α are shown in Figure 3.

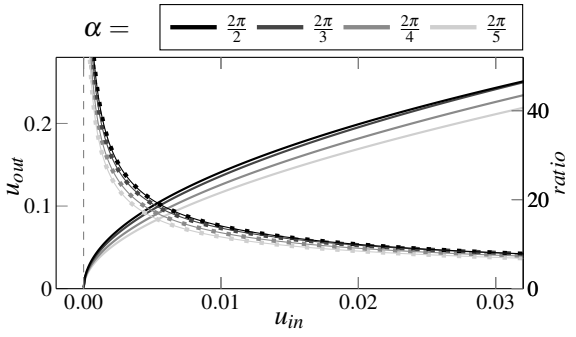

FIGURE 3. Transmission behavior of a unit cell. Output displacement, represented by thick lines, and transmission ratio, represented by thin lines with square markers. Input and output displacements shown as fractions of link length l.

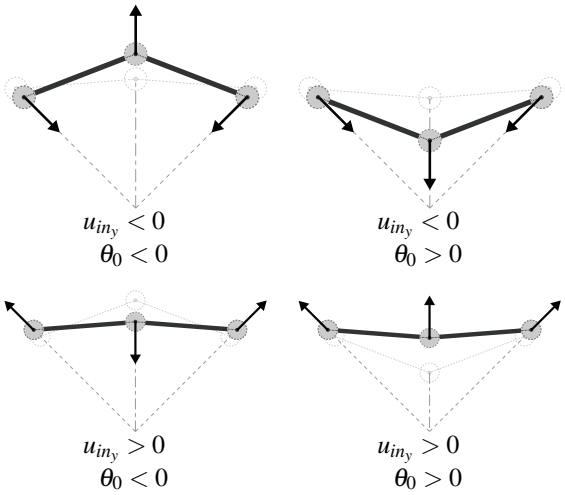

FIGURE 4. Input/output modalities of a single amplification stage.

It can be seen that for small strokes, in the lower percentage regime of the link length, smaller normal angles yield higher transmission ratios.

Depending on the initial angle θ_0 of the links and the direction of u_{in}, different input/output modalities can be achieved. The set of possible configurations is shown in Figure 4. Unit cells with pushing input nodes ($u_{in_y} < 0$) possess decreasing transmission ratios while unit cells with pulling input nodes ($u_{in_y} > 0$) possess increasing transmission ratios. By combining multiple amplification stages with different modalities in series, 4^{n_s} mechanism configurations can be achieved which exhibit complex transmission behaviors.

Constrained rigid link concept

Intermediate hubs are added at the interface to the mechanism input and output, as well as between amplification stages. In order to fix the relative rotations between the hubs, the single links of the basic concept are substituted by parallelogram linkages. This is shown in Figure 1 b).

Compliant concept

In the last step, the constrained rigid link mechanism is approximated by a compliant mechanism, in which the rotational degrees of freedom are obtained by bending of compliant links, that substitute both the rigid links and the revolute joints. This step is shown in Figure 1 c).

PARAMETRIZATION

The parametrization of the mechanism is done on the basis of the unit cells, representing each amplification stage, as shown in Figure 5.

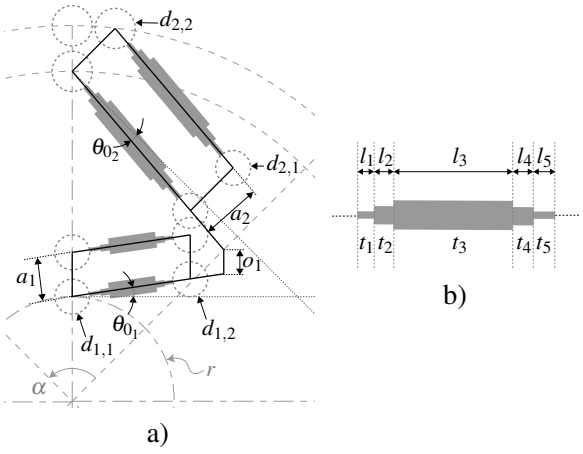

FIGURE 5. Mechanism parametrization.

Due to the mirror symmetry along the unit line, only one side is considered. Each unit cell is defined by four parameters. Its layout is described by the neutral axes of the compliant links, as is illustrated in Figure 5 a).
A parallelogram is given by the inner radius r, the normal angle α, the angle θ_0, and by the offset a between the two parallel lines. The total length of the compliant links is determined by this parallelogram description and the connector diameters d that define the margin for the intermediate hubs at each end. Two adjacent stages are separated by an offset o that determines the distance between the inner beams of both stages, such that their end nodes do not coincide. This distance is defined orthogonally to the singularity line of the inner stage.
The compliant links of each stage, are modeled by a chain of rigidly interconnected beam elements, each of which has a parameter defining its relative length l and its thickness t. This is shown in Figure 5 b). All stages and beams are indexed from output to input of the mechanism.

OPTIMIZATION

In order to obtain a feasible mechanism with an optimal transmission ratio, an optimization routine is conducted to find the ideal parameters.
The full parameter set $\mathbf{x}$ is given by:

$$\begin{aligned}\mathbf{x} = [\quad & [\Psi],\ [n_n], \\ & [\theta_1, \ldots, \theta_{n_s}], \\ & [s_1, \ldots, s_{n_s}],\ [a_1, \ldots, a_{n_s}], \\ & [o_1, \ldots, o_{n_s-1}],\ [d_{1,1}, \ldots, d_{n_s,2}], \\ & [t_{1,1}, \ldots, t_{n_s,n_b}],\ [l_{1,1}, \ldots, l_{n_s,n_b}] \quad]\end{aligned} \tag{2}$$

The parameter Ψ is a binary value and controls the actuation direction at the input, while n_b marks the number of beam elements that form one compliant link. In the scope of this investigation, only mechanisms that are composed of two stages are considered ($n_s = 2$). Each compliant link is discretized by five beam elements, thus $n_b = 5$. Hence, the total number of parameters is 33.

The objective $\boldsymbol{\delta}$ of the optimization is to maximize the output force F_{out} for a given input force F_{in} and input stroke Δu_{in}. Thus, $\boldsymbol{\delta}$ becomes the inverse of the output force.

$$\boldsymbol{\delta} = {F_{out}}^{-1} \tag{3}$$

Geometric constants for the shaft diameter, brake shoe thickness and initial air gap between the aforementioned are prescribed, determining the inner radius r and the output stroke Δu_{out} before contact. A soft constraint on the maximum stress σ_{max} is given in the form of a penalty $\mathbf{p}$, which is multiplied by a penalty factor k_p and added to the objective. The minimization problem becomes:

$$f(\mathbf{x}) = \boldsymbol{\delta} + k_p \mathbf{p} \tag{4}$$

All parameters in $\mathbf{x}$ are subject to upper bounds $\mathbf{b_u}$ and lower bounds $\mathbf{b_l}$. Furthermore, sets of linear inequality constraints $\mathbf{c_l}$ and non-linear inequality constraints $\mathbf{c_{nl}}$ are used to ensure the geometrical feasibility of candidate geometries.

Optimization Model

The flexible multibody dynamics software package SPACAR [11] is used to simulate one unit cell of the fully parametrized mechanism, as is shown in Figure 6. The compliant links are modeled using flexible finite two-node planar beam elements. Intermediate bodies, such as the hubs and the brake shoe, are modeled using rigid beam elements. The shaft is modeled using a beam element with stiffness properties corresponding to the shaft diameter. These beam elements include geometric nonlinearities and their flexibility is formulated in the form of discrete deformation modes. Symmetry conditions are applied to the two nodes intersecting with each normal-line, respectively. Thereby, their radial and circumferential translations as well as their rotations are positively and rigidly coupled.

Optimization Procedure

For each candidate parameter set, a two-step kinetostatic simulation is executed. First, the normal force F_n acting on the shaft is evaluated,

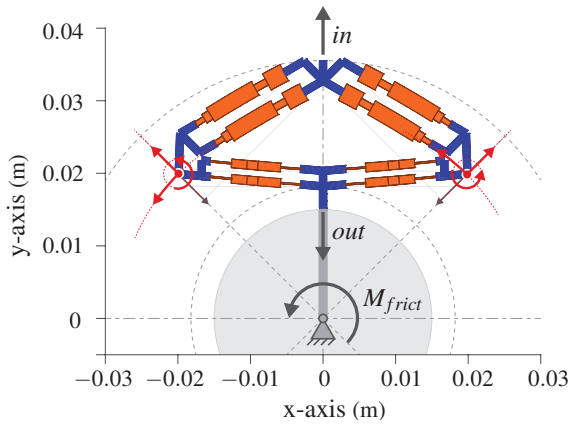

FIGURE 6. Optimized unit cell geometry. Flexible beams drawn in orange, rigid beams in blue and the shaft beam in gray. The gray field indicates the shaft diameter. Gray arrow symbols show load directions. Red arrow symbols show symmetry conditions.

considering the contact between brake shoe and shaft. Consecutively, a moment M_{frict} is applied at the shaft's central rotation axis, which represents the maximum static moment that the mechanism can hold based on F_n and assuming a friction coefficient μ. This results in an added tangential force component F_t at the brake shoe, leading to a small decrease of the applied normal force F_n. This reduced normal force between brake shoe and shaft yields the operational output force F_{out}, which determines the objective value $\boldsymbol{\delta}$. Further, the maximum stress σ_{max} in the compliant beams is determined for this combined load case, yielding the penalty value $\mathbf{p}$. The Genetic Algorithm function ga() from the MATLAB Global Optimization Toolbox is used, for solving the minimization problem.

RESULTS

For an input force $F_{in} = 1750$ N, and input displacement $\Delta u_{in} = 20$ µm, a shaft diameter of 30 mm, a brake shoe thickness of 3 mm, an initial air gap (Δu_{out}) of 200 µm, a friction coefficient of $\mu = 0.5$, and using a AISI 420 tool steel ($E = 200$ GPa, $G = 80$ GPa, $\sigma_{yield} = 1280$ MPa) a design is obtained that can provide a holding torque of up to 1.9 Nm. The resulting unit cell geometry is the one shown in Figure 6. The kinetostatic transmission behavior from input to output regarding radial position and forces can be seen in Figure 7 and Figure 8, respectively. The graphs show that the transmission behavior can be roughly described as piecewise linear, having straight segments for the non-contact and the

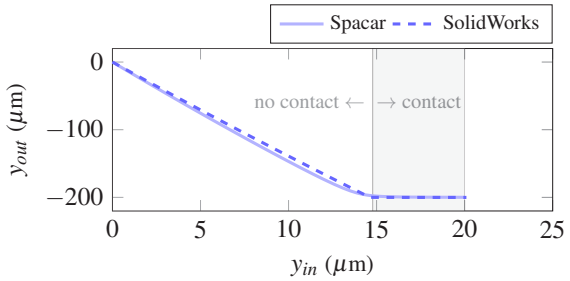

FIGURE 7. Displacements of the unit cell.

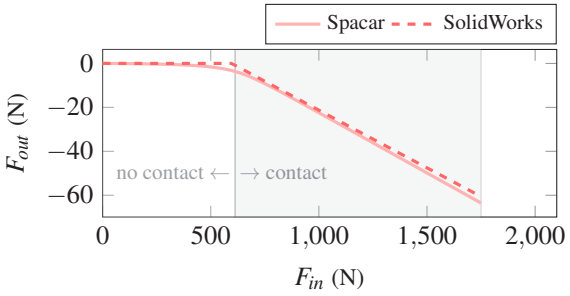

FIGURE 8. Force transmission of the unit cell.

contact region. The transmission ratio before contact as determined by the displacements is -14.1, the ratio after contact as determined by the forces is -18.7. The entire mechanism has an outer diameter of 69.96 mm and is 10 mm in height.

Validation

The mechanism was modeled, as is shown in Figure 9, and analyzed using a non-linear static contact analysis in the SolidWorks Simulation toolbox. The results are shown along with the SPACAR results in Figure 7 and Figure 8. Both, the displacements and the forces show good agreement. The maximum stress is found to be 313 MPa in SolidWorks and 338 MPa in SPACAR.

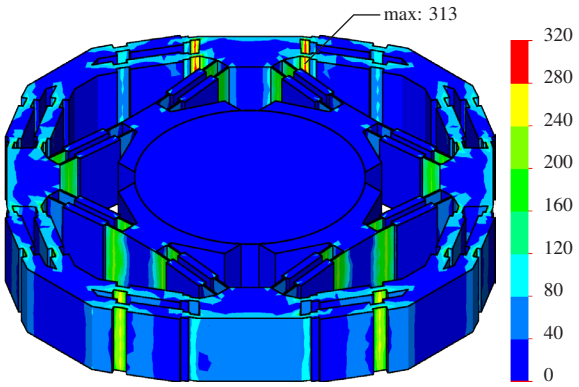

FIGURE 9. SolidWorks simulation stress plot. Stresses shown in MPa.

DISCUSSION

The concept investigated in this paper is limited to polygon shaped node arrangements with $n_n \geq 3$ inputs. However, given a different mechanism layout, designs with $n_n = 2$ inputs are also feasible, allowing a normal angle of $\alpha = \pi$.

In order to eliminate any under-constraints, the input nodes are required to be translationally and rotationally constrained in all planar directions.

The proposed actuation via PZT-stacks can be done in various manners. Two possible methods are direct actuation in which each input is actuated by a separate, dedicated PZT-stack, and actuation by an out-of-plane flexure mechanism which transforms a single axial displacement into a distributed radial displacement at the inputs. Also integrating piezo-stacks into the planar mechanisms rigid sections appears feasible.

The presented mechanism can be converted into a normally closed version, by using its fully deflected shape at full input displacement, not considering the contact, as the initial shape and inverting the input direction.

The small deviation between the force profiles of the SPACAR model and the SolidWorks model may be caused by the deformation of the intermediate bodies, which were assumed perfectly rigid in the SPACAR model.

CONCLUSION

This paper presents a synthesis method to obtain compliant planar mechanisms, which can be used to clamp a centrally located shaft. The distinctive features are the monolithic design and the achievable high motion amplification ratio, making the use of PZT-stack actuators with micrometer scale input strokes feasible. The proposed optimization routine is applied and yields a compact mechanism design, that can transform a 1750 N and 20 µm actuator input into a 1.9 Nm braking torque, after traveling across an air gap of 200 µm. The results are successfully validated across different software packages.

ACKNOWLEDGMENTS

This project has received funding from the European Union's Horizon 2020 research and innovation programme under grant agreement No. 688857 (SoftPro).

REFERENCES

[1] Plooij M, Mathijssen G, Cherelle P, Lefeber D, Vanderborght B. Lock Your Robot: A Review of Locking Devices in Robotics. IEEE Robotics Automation Magazine. 2015;22.

[2] Leal Jr AG, de Andrade RM, Filho AB. Series Elastic Actuator: Design, Analysis and Comparison. Recent Advances in Robotic Systems. 2016;.

[3] Haeufle DFB, Taylor MD, Schmitt S, Geyer H. A clutched parallel elastic actuator concept: Towards energy efficient powered legs in prosthetics and robotics. In: 4th IEEE RAS EMBS International Conference on Biomedical Robotics and Biomechatronics (BioRob); 2012. p. 1614–1619.

[4] Wolf S, Grioli G, Eiberger O, Friedl W, Grebenstein M, Hppner H, et al. Variable Stiffness Actuators: Review on Design and Components. IEEE/ASME Transactions on Mechatronics. 2016 Oct;21(5):2418–2430.

[5] Plooij M, Wolfslag W, Wisse M. Clutched Elastic Actuators. IEEE/ASME Transactions on Mechatronics. 2017 April;22(2):739–750.

[6] Schmid SR, Hamrock BJ, Jacobson BO. Fundamentals of Machine Elements. CRC Press; 2014.

[7] Yamatoh K, Ogura M, Kanbe K, Isogai Y. Piezoelectric brake device. Google Patents; 1987. Patent US07182964.

[8] Hanley MG, Caliendo GP, Anderson DB. Actuator having piezoelectric braking element. Google Patents; 1997. Patent US5986369.

[9] Ling M, Cao J, Zeng M, Lin J, Inman DJ. Enhanced mathematical modeling of the displacement amplification ratio for piezoelectric compliant mechanisms. Smart Materials and Structures. 2016;25(7):075022.

[10] Hoberman C. Radial expansion/retraction truss structures. Google Patents; 1988. Patent US5024031A.

[11] Jonker JB, Meijaard JP. In: Schiehlen W, editor. SPACAR — Computer Program for Dynamic Analysis of Flexible Spatial Mechanisms and Manipulators. Springer Berlin Heidelberg; 1990. p. 123–143.